Available online at www.sciencedirect.com
ScienceDirect
Trans. Nonferrous Met. Soc. China 31(2021) 3929−3942
Transactions of Nonferrous Metals Society of China
www.tnmsc.cn

Evaluation of cathode quality and damage of aluminium electrolytic cell based on non-destructive technology

Yu LUO[1], Sheng-xiang LI[1], Dao-long CHEN[1], Xi-ling LIU[1], Chun-de MA[2], Xi-bing LI[1]

1. School of Resources and Safety Engineering, Central South University, Changsha 410083, China;
2. Advanced Research Center, Central South University, Changsha 410083, China

Received 20 November 2020; accepted 8 September 2021

Abstract: To evaluate the quality and damage condition of the electrolyzer, wave velocity detection technology and impact echo technology were used to detect the cathode part of the electrolyzer. The experimental results show that wave velocity is linearly related to the porosity, and there is also a linear relationship between wave velocity and the square root of reciprocal density in cathode carbon blocks (CCBs) before installation into electrolyzer. Combined with detection results of wave velocity and voltage drop, the large-size CCBs with relatively good quality can be found. Through the impact echo technology on cathode steel rods (CSRs), the results of the on-site detection show that the damage condition of CSRs can be effectively evaluated, and the damage location of CSRs can be determined. This study proposes a novel and quantifiable method for the evaluation of cathode quality and damage, which provides a reference for prolonging the service life of the electrolyzer.

Key words: electrolyzer; wave velocity detection; impact echo technology; cathode quality; damage evaluation

1 Introduction

The electrolyzer is the core equipment in the production process of aluminium electrolysis, and its service life is a comprehensive symbol of electrolytic aluminium technology and economy. The cathode carbon block at the bottom of the electrolyzer is the most important component. When cathode carbon blocks (CCBs) are seriously damaged, the high-temperature aluminium liquid contacts with cathode steel rods (CSRs) through CCBs and chemically reacts with irons, resulting in an increase of iron content in molten aluminum. As a result, the service life of the electrolyzer will be shortened, and potential safety hazards and economic losses can be caused [1−6].

Since the quality of CCBs strongly affects the service life of the electrolyzer, it is of great importance to evaluate the quality of CCBs before installation into the electrolyzer. At present, the method of sampling surveys has been widely used in the quality inspection of CCBs in the electrolytic aluminium industry to detect the physical, chemical and mechanical index of the CCB samples, while the detection of internal defects is not required. The acoustic detection method can be applied to evaluating the quality of CCBs. In the late 1960s, some researchers began to study the relationship between the ultrasonic propagation velocity and the pore size of graphite products by ultrasonic detection [7]. Through continuous research, the linear correlation between the quality of CCBs at the bottom and carbon crucible for molten metal controlled by ultrasonic was obtained. The frequency dependence of attenuation coefficients of graphite material was measured, and the distance−amplitude characteristic curves of some artificial

Corresponding author: Xi-ling LIU, Tel: +86-18607311798, E-mail: lxlenglish@163.com
DOI: 10.1016/S1003-6326(21)65775-8

defects of graphite material were obtained [8,9]. Further, the relationship between the ultrasonic wave velocity and the structural defects in the carbon block was developed [10]. Subsequently, ultrasonic testing has been used to evaluate the quality of CCBs before the installation into the electrolyzer. In this way, the wave velocity can match the physicochemical indicators and strength, and internal defects of CCBs can be reflected clearly. The ultrasonic testing also has the advantages of simple equipment, flexible use, and portability.

To evaluate the damage condition of the cathode during the operation of the electrolyzer, iron content detection of aluminium melts, temperature detection of CSRs, abnormal detection of cathode voltage drop have been widely adopted. However, these detection methods cannot accurately locate the damaged parts or evaluate the damage degree without reference standards. Besides, these detection methods can only detect the late stage of damage rather than the early stage of damage [11−17]. During the operation of the electrolyzer, CCBs are under high-temperature aluminium melt and are enclosed in the electrolyzer, while CSRs protrude out of the electrolyzer. If the non-destructive testing method can be used to detect the damage condition of CSRs and determine the damage location of CSRs through the outcrop area, the integrity of CSRs can be effectively evaluated in time, and the corresponding repairs can be made. Generally, internal defects in steel rods can be detected through ultrasonic non-destructive testing [18−23]. However, due to the limitation of site conditions such as electromagnetic field interference, it is difficult to detect the damage condition and location of CSRs by the ultrasonic method in the running electrolyzer. In addition, the high-frequency signals used in the ultrasonic method cannot propagate a long distance in CSRs eroded by high-temperature aluminium melts, which affects the detection accuracy. Therefore, the detection of CSRs in the electrolyzer requires a low frequency and good penetration signal technology, and the impact echo detection technology is an appropriate method. Impact echo detection technology has been widely employed to detect the internal structural defects of materials, such as the detection of internal voids in the wood [24−26], the integrity detection of pile foundations [27], the detection of internal defects in concrete [28], the detection of internal defects in rocks [29], and the thickness measurement of the refractory wall of blast furnace wall [30−32]. If the damage condition and location of the cathode of the electrolyzer can be detected by the impact echo method, the potential safety hazards of cathode damage will be solved, and significant economic benefits can be brought to the electrolytic aluminum enterprises. Therefore, it is a meaningful pursuit to detect the damage of CSRs by the impact echo method.

In this study, ultrasonic testing technology was used to evaluate the quality of CCBs before installation into the electrolyzer, and the relationship between the wave velocity and the conventional quality evaluation indexes of CCBs such as porosity and density were established. Besides, the impact echo detection technology was used to detect the damage condition and location of CSRs of the electrolyzer, and the application effect of the test was evaluated. This provides a fast and effective technical scheme for the quality evaluation of CCBs in the electrolyzer.

2 Experimental

2.1 Wave velocity detection scheme of CCBs before installation into electrolyzer

The semi-graphite CCBs (marked as C1 and C2) were used for wave velocity detection in this study. The C1 and C2 samples were produced by two different companies and have been used by the Chongqing Qineng Electrolytic Aluminium Plant in China. The CCBs were made of anthracite, graphite scrap, asphalt and other raw materials through batching, calcination, compression, calcination, graphitization and other processes. According to the material testing standards established by ASTM, the carbon cores were taken from the complete CCBs and processed into a cylindrical specimen of d50 mm × 100 mm, and the acoustic testing instrument RSM-SY5 (Institute of Rock and Soil Mechanics, Chinese Academy of Sciences) was used to measure the wave velocity. An acoustic wave signal with an excitation frequency of 50 kHz was generated in the sample axis, and the propagation time of the excitation signal in the CCB was measured and repeated three times to calculate the mean value of wave velocity.

Subsequently, the density (ISO 12985-1:2000), porosity, strength (ISO 18515:2007), resistivity (ISO 11713:2000), ash content (ISO 8005:2005) and other indicators of CCB samples were measured by the electronic weighing, Vernier calliper, rock nuclear magnetic resonance imaging system, electro-hydraulic servo universal testing machine and other instruments, respectively. Except for compressive strength, the mean values of indicators were calculated after three repeated tests. In addition, the electrometer voltmeter (PRS-200T, Qingdao Prius Electrical Equipment Co. Ltd., China) and the acoustic testing instrument (RSM-SY5) were used to conduct a full detection range of voltage drop and wave velocity on the complete CCBs, and the mean values of wave velocity and voltage drop were calculated after repeated three tests. Five samples were selected from each type of CCBs and marked as C1-1−C1-5, and C2-1−C2-5. Figure 1 shows the measurement points of CCBs.

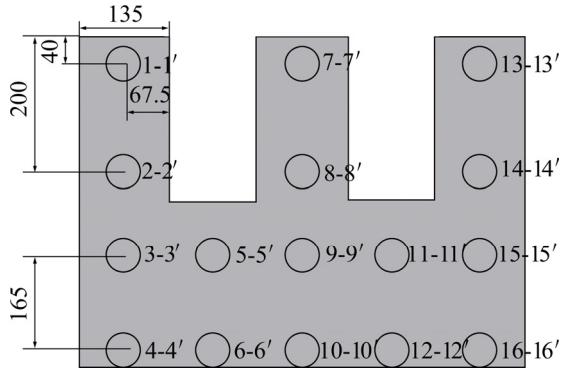

Fig. 1 Measurement points for wave velocity and voltage drop on main view of CCB specimens (unit: mm)

2.2 Impact echo testing scheme on CSRs in running electrolyzer

The main principles of the impact echo method are as follows. A mechanical point impact on the surface of the elastomer is applied by a steel ball or hammer, and a sensor is installed near the impact position; then the reflected energy is recorded as a time-domain waveform and simultaneously converted into frequency-domain waveform by the Fourier transform; the time-domain waveform and the frequency-domain waveform are jointly used to identify defects in materials [33]. As shown in Fig. 2, when the excitation device impacts the top of CSR, the vibration is generated and propagated in the form of stress waves. If a defect is encountered, the accelerometer at the top of the CSR receives a partial reflection echo at the defect; thus, the location and properties of the defect can be determined according to the arrival time and phase of the echo. The rest of the stress wave propagates to the bottom of the CSR and is reflected back.

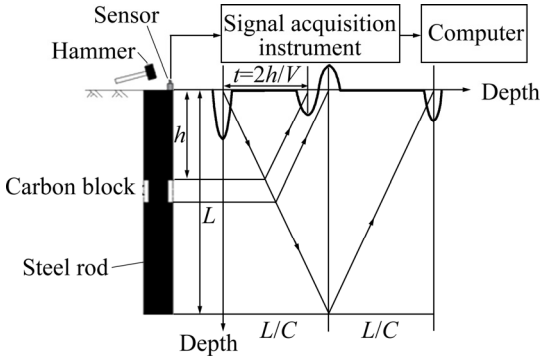

Fig. 2 Schematic of impact echo method

In this study, the impact echo device RS−1616 (KS) was used to detect CSRs in the damaged electrolyzer in the production workshop of the above-mentioned aluminium factory. The sensitivity of the accelerometer was 100 mV/g, the range was 50*g* (where *g* denotes the gravity acceleration), and the resonance frequency was 27 kHz. A total of 10 CSRs (numbered as A1−A10) were tested on-site; the length of the CSR sample was 2.2 m, the size of the rectangular section was 100 mm × 200 mm. Because the lower part of CSR was connected with the cathode bus, the upper part of CSR was the only section that can be used for impact echo detection, and the cross-section of its outcrop was 200 mm × 20 mm. Considering the little length of CSRs and the influence of the electromagnetic field, a copper hammer was used for excitation [34]. In the process of excitation, it should be ensured that there was no significant difference in the impact force each time. The excitation point and the position of the accelerometer were respectively arranged at one-third of the length of the CSR outcrop.

3 Results and discussion

3.1 Wave velocity detection of CCBs before installation into electrolyzer

The propagation velocity of elastic waves in materials is closely related to defects in the structure, material density, and elastic modulus [35]. In the theory of elastic wave propagation, the

longitudinal wave velocity can be determined by the following formula [36]:

$$V_{\mathrm{p}}=\sqrt{\frac{E(1-\mu)}{\rho(1+\mu)(1-2\mu)}} \tag{1}$$

where V_{p} is the longitudinal wave velocity (m/s); E is the elastic modulus (MPa); ρ is the bulk density (g/mm^3); μ is the Poisson's ratio.

Therefore, if there are many pores and cracks in CCBs, the elastic wave propagation velocity will be significantly reduced; if large changes of wave velocity are detected in different parts of the same CCB, the CCB is not homogeneous. Based on the above theory, the quality of CCBs can be evaluated.

3.1.1 Wave velocity and physicochemical indicators of CCB specimens

The relationship between the wave velocity, porosity, and square root of the reciprocal density of the two types of CCBs is shown in Fig. 3, and the specific values of various indicators are listed in Table 1. With the decrease of apparent density and the increase of porosity, the ultrasonic propagation velocity decreases continuously, and the porosity, and square root of reciprocal density are linearly related to the ultrasonic propagation velocity, respectively. For the same type of CCBs, the higher the density is, the less the pores are, and the higher the ultrasonic propagation velocity is. The results show that it is feasible to use wave velocity to evaluate the homogeneous quality of CCBs.

As shown in Fig. 3, the wave velocity of C2 is greater than that of C1, indicating that the wave velocity is also related to the type of CCB raw material and the manufacturing process.

3.1.2 Relationship between wave velocity and voltage drop in intact CCBs

Based on the above results, the tests are conducted on CCBs according to the scheme in

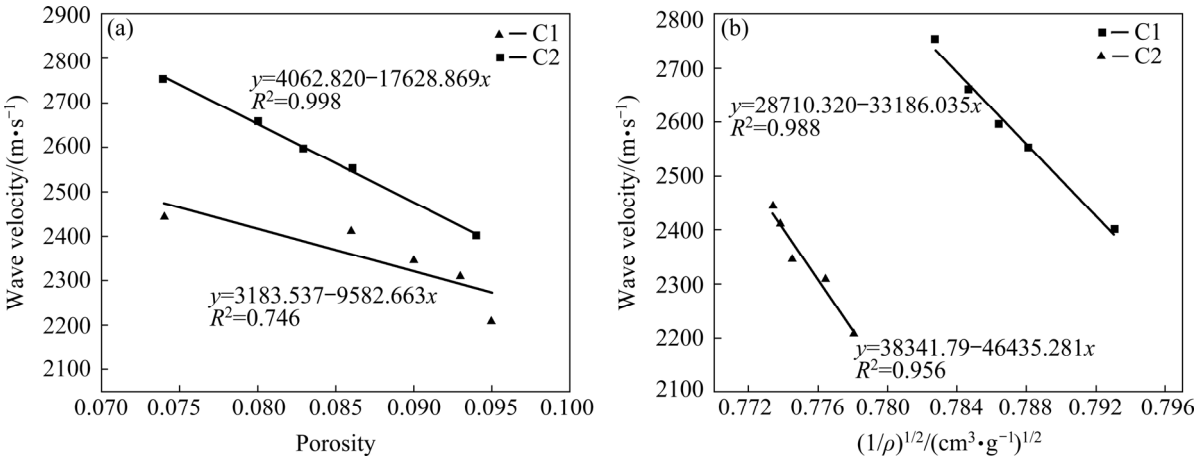

Fig. 3 Relationship between wave velocity and porosity (a) and square root of reciprocal density (b) of CCB specimens

Table 1 Wave velocity and physicochemical indicators of C1 and C2 specimens

Specimen	Wave velocity/ (m·s^{-1})	Density/ (g·cm^{-3})	Porosity	Resistivity/ (μΩ·m)	Ash content/%	Compressive strength/MPa
C1	2209.186	1.652	0.095	24	3.13	25.374
	2308.621	1.659	0.093	28	2.80	27.210
	2346.203	1.667	0.090	28	2.82	29.988
	2412.185	1.670	0.086	31	2.63	33.077
	2444.282	1.672	0.074	33	2.50	38.848
C2	2400.931	1.590	0.094	45	3.74	33.719
	2553.117	1.610	0.086	47	3.49	33.854
	2596.964	1.617	0.083	44	3.41	29.697
	2659.656	1.624	0.080	49	3.35	34.943
	2752.192	1.632	0.074	48	3.26	35.030

Fig. 1. The test results of wave velocity and voltage drop of C1 and C2 specimens are given in Table 2 and Table 3. In this study, 80 measuring points in the main view of C1 are used to analyze the variation of wave velocity and voltage drop. As shown in Fig. 4(a), the wave velocity of C1 is distributed in the range of 2300−2700 m/s. The proportion of data distributed below 2400 m/s is small, while the proportion of data in the range of 2400−2700 m/s is dominated, accounting for approximately 98.75%. It is worth mentioning that the wave velocity at measurement points 12-12′ of C1-3 deviates greatly from these values. As presented in Table 2, the standard deviation and the deviation between minimum and average of C1-3

Table 2 Wave velocity calculation results of C1 and C2 CCBs

Specimen	Average velocity/(m·s^{-1})	Standard deviation	Deviation between minimum and average/(m·s^{-1})
C1-1	2611.970	11.060	26.470
C1-2	2494.530	34.720	62.530
C1-3	2456.530	32.560	90.030
C1-4	2626.880	17.740	44.380
C1-5	2544.590	32.300	76.590
C2-1	2786.060	29.790	53.060
C2-2	2766.810	26.720	52.810
C2-3	2747.060	22.730	30.060
C2-4	2761.380	33.360	55.380
C2-5	2794.970	19.040	43.470

Table 3 Voltage drop calculation results of C1 and C2 CCBs

Specimen	Average voltage drop/mV	Standard deviation	Deviation between maximum and average/mV
C1-1	45.37	5.22	−7.34
C1-2	48.13	6.66	−9.77
C1-3	46.21	5.93	−8.54
C1-4	43.39	4.62	−6.76
C1-5	47.45	5.94	−8.86
C2-1	72.71	7.15	−10.16
C2-2	69.01	7.27	−10.22
C2-3	66.47	6.83	−10.07
C2-4	70.60	6.71	−8.82
C2-5	67.31	7.51	−11.60

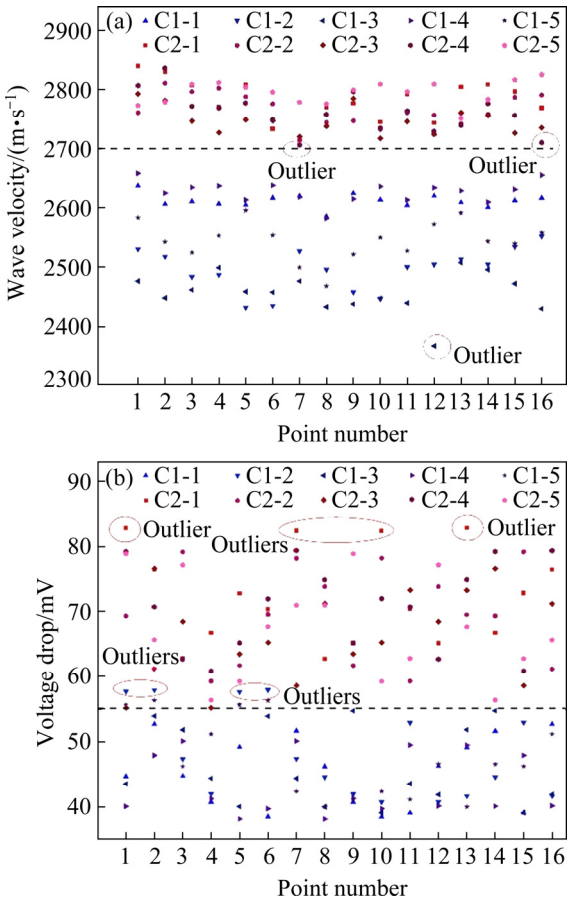

Fig. 4 Distribution of wave velocity (a) and voltage drop (b) of CCBs

are relatively large, indicating that the C1-3 specimen has a poor homogeneity; the wave velocity of C1-3 at the measuring point 12-12′ is only 2366.5 m/s. Besides, C1-1 and C1-4 have higher wave velocity and smaller standard deviation, indicating that C1-1 and C1-4 specimens have good homogeneity and quality, while C1-2 and C1-5 have higher wave velocity but larger standard deviation, indicating that C1-2 and C1-5 specimens have poor homogeneity.

As shown in Fig. 4(b), the voltage drop of C1 specimens is mainly distributed in the range of 35−60 mV, and the amount of data with the voltage drop beyond 55 mV is small. The values of voltage drop in the range of 35−55 mV are dominated, accounting for 90% of the total data. However, the voltage drops at measurement points 1-1′, 2-2′, 5-5′, 6-6′ of C1-2 and C1-5 deviate greatly from the dominated values. As shown in Table 3, for C1-2 and C1-5 specimens, the standard deviation and the deviation between the maximum value and average are relatively large, indicating that C1-2 and C1-5

have poor homogeneity, and their voltage dropped at the measuring point 1-1′, 2-2′, 5-5′ and 6-6′ exceed 55 mV. The voltage drop and the standard deviation of C1-1, C1-3 and C1-4 are small, indicating that these specimens have better homogeneity. In the actual production process, the resistance value of the upper part of CCBs (the unslotted part) is more important, and it can be considered that the measured resistance value of C1 specimens conforms to the requirements.

As shown in Table 1, the wave velocity, voltage drop and physicochemical properties of the two types of CCBs are quite different. Specifically, C1 has the lower ash content, resistivity, voltage drop, strength and wave velocity, but the higher porosity; while C2 has the higher ash content, resistivity, voltage drop, wave velocity and strength, but the lower porosity. The above analysis shows that the combined test of wave velocity and voltage drop can effectively evaluate the quality of each CCB before installation into the electrolyzer and compare the properties of different types of CCBs.

3.2 Impact echo damage detection of CSRs in running electrolyzer

Based on the damage condition of CSRs in the electrolyzer in the previous studies, the damage degree of CSRs can be divided into three categories: (1) Type I CSR has minor surface damage but good integrity; (2) Type II CSR is partially melted without the penetrating cracks, and the cross-sectional area of the melted area is smaller than the original area; (3) Type III CSR is penetrated by cracks. Based on the results obtained by the impact echo method, the integrity of CSRs can be comprehensively determined by wave velocity inversion analysis, time−frequency domain analysis and amplitude attenuation characteristic analysis.

3.2.1 Wave velocity inversion analysis

Previous studies [37−39] have shown that the faster the wave velocity of the stress wave in the material is, the better the integrity is. Through the inversion of the wave velocity in CSRs, the damage condition can be preliminarily judged. Because the length of CSRs in service is 2.2 m, the wave velocity in the three types of CSRs can be calculated according to the original length of CSRs and the time difference between the incident wave and the reflected echo on the time-domain curve. In this study, the wave velocity in Type I CSR is calibrated, and its wave velocity is taken as the reference value, and then the difference between the wave velocity and the reference value in each CSR is compared to evaluate its damaged condition. To determine a reference value for the wave velocity, the impact echo test is conducted on a 1.90 m-long CSR before installation into the electrolyzer. The test results are shown in Fig. 5. The stress wave has multiple reflections at the top and bottom ends of the CSR, and the time intervals between two adjacent peaks in the time-domain are approximately equal, and the amplitude gradually attenuates. The calculated wave velocity is 4798 m/s, which can be used as a reference value.

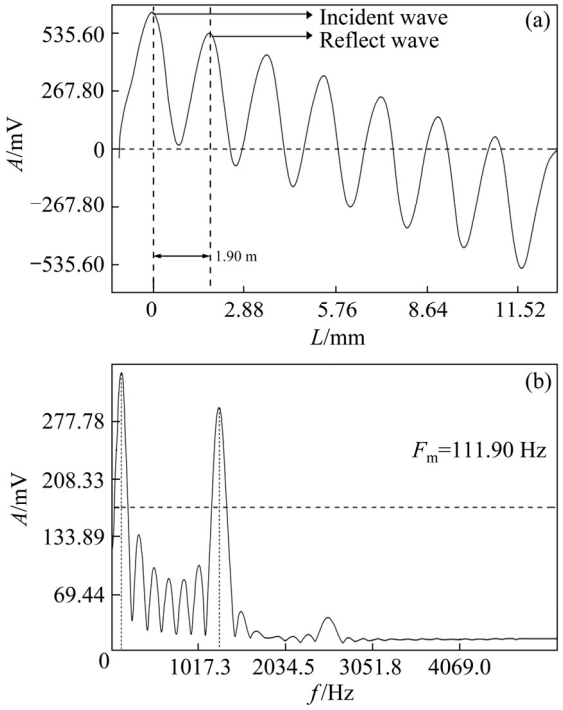

Fig. 5 Time−frequency domain waveform detected in Type I CSR before installation into electrolyzer (Test site: Maintenance workshop; Wave velocity: 4798 m/s): (a) Time domain; (b) Frequency domain

Table 4 gives the calculated wave velocities of various on-site CSRs. There are significant differences in wave velocities among the three types of CSRs. Specifically, Type I CSRs have better integrity, and the wave velocity is closer to that of the reference value. Type II CSRs have defects and the calculated wave velocity is lower than the reference value. This is because the defects are filled with impurities such as electrolyte and aluminium liquid, and the stress wave propagates or

Table 4 Inversion results of stress wave velocity

Specimen	Wave velocity/(m·s^{-1})	Damage category
A1	4825	I
A2	5093	I
A3	5093	I
A4	5473	I
A5	5641	I
A6	5820	I
A7	3107	II
A8	2026	II
A9	11111 (abnormal)	III
A10	11828 (abnormal)	III

diffracts in the impurities to cause low values. Type III CSRs are fused, resulting in a shorter propagation distance of the stress wave, and the calculated wave velocity based on the actual length of the CSR (2.2 m) is abnormally larger than the reference value.

When the stress wave propagates in the medium, the energy of the elastic wave is dissipated by geometrical spreading, internal friction, mode conversion and scattering. Stress wave parameters such as amplitude and frequency decrease with the increase of propagation distance, which is called stress wave attenuation [40]. In impact echo detection, due to the attenuation of the stress wave energy in CSRs, the energy of the reflected wave signal is far less than that of the incident wave. Therefore, the measured amplitudes of the incident wave and reflected wave are used to calculate the attenuation coefficient in CSRs, and the relationship between attenuation coefficient and wave velocity is used to verify the reliability of inversion wave velocity. Equation proposed by FUTTERMAN [41] is used to calculate the attenuation coefficient:

$$A_2 = A_1\exp(-\alpha\Delta x) \quad (2)$$

where α is the attenuation coefficient; Δx is the propagation distance; A_1 is the amplitude of stress wave reflected from the top of CSRs; A_2 is the amplitude of stress wave reflected from the bottom of CSRs.

The wave velocity and the attenuation coefficient of Type I CSRs are listed in Table 5. Figure 6 shows the time-domain curves of CSRs listed in Table 5. Figure 7 shows the relationship between wave velocity and attenuation coefficient, and Fig. 8 also depicts the time−frequency domain waveform of some CSRs listed in Table 5. As shown in Fig. 7, there is a linear correlation between wave velocity and the attenuation coefficient of Type I CSRs. The smaller the wave velocity is, the greater the attenuation coefficient is, and the more serious the damage of CSRs is. Besides, the attenuation coefficient can be used to verify the wave velocity in the time-domain analysis of Type I CSRs. Table 6 gives the wave velocity verified by the attenuation coefficient, the inversion wave velocity and their percentage difference. The difference between the verified wave velocity and the inversion wave velocity is not more than 3%, indicating that the inversion wave velocity is reliable.

3.2.2 Time and frequency domain analysis

In this study, all time-domain waveforms were detected, and the spectrum of each time-domain waveform is realized by the fast Fourier transform (FFT). Through a comprehensive analysis of the time and frequency domain analysis, the damage degree of CSRs can be evaluated. Due to the different stress wave velocities and different damage degrees of CSRs, the wave velocity in CSRs should be estimated before the location and defect analysis. When the reflected waves at the

Table 5 Wave velocity and attenuation coefficient of stress wave of Type I CSRs

Specimen	Amplitude, A_1/ mV	Amplitude, A_2/mV	Propagation distance, Δx/m	Wave velocity/ (m·s^{-1})	Attenuation coefficient
A1	636.52	149.54	4.40	4825.00	0.329
A2	286.09	73.77	4.40	5093.00	0.308
A3	533.89	138.78	4.40	5093.00	0.306
A4	572.20	169.66	4.40	5473.00	0.276
A5	217.12	63.48	4.40	5641.00	0.279
A6	530.87	164.99	4.40	5820.00	0.266

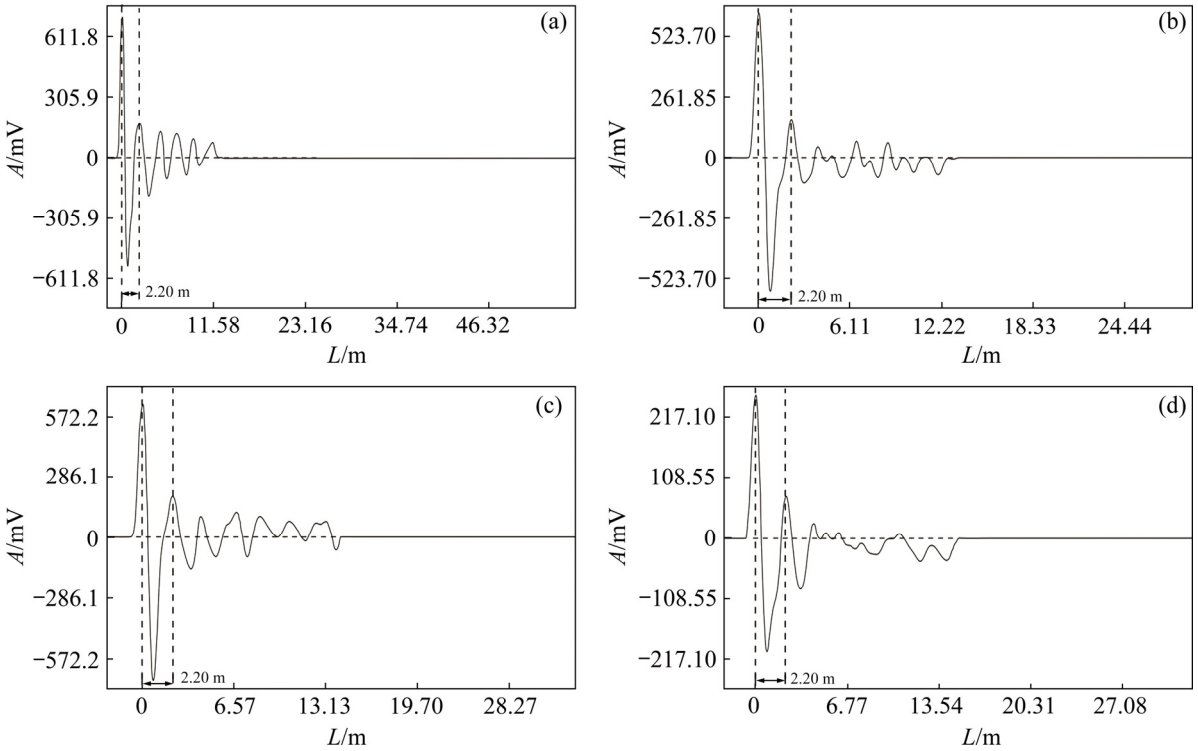

Fig. 6 Time-domain curve diagrams of Type I CSRs: (a) Al (Wave velocity: 4825 m/s); (b) A3 (Wave velocity: 5093 m/s); (c) A4 (Wave velocity: 5473 m/s); (d) A5 (Wave velocity: 5641 m/s)

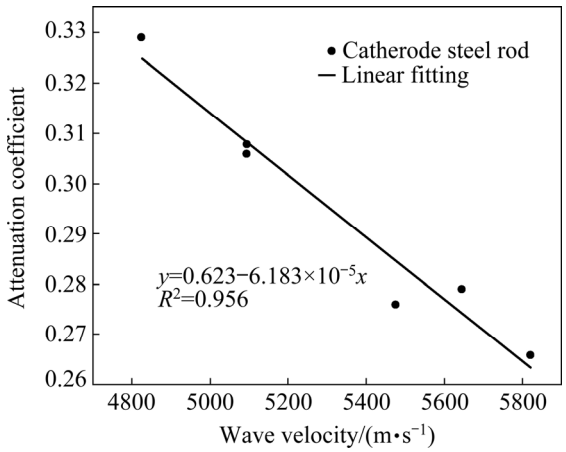

Fig. 7 Relationship between wave velocity and attenuation coefficient of Type I CSRs

bottom of CSRs are relatively clear, the wave velocities can be calculated based on the length of CSRs and the arrival time of reflected echo. When the reflection echo at the bottom of CSRs cannot be determined, the stress wave velocity of Type I CSRs is considered as a reference (see Section 3.2.1).

The basic theories of time−frequency domain analysis are available in references [42,43]. Assuming that CSR is a one-dimensional elastic rod with uniform and continuous medium, the cross-section remains flat during the longitudinal vibration, the axial stress on the cross-section is evenly distributed, the incident wavelength is much greater than the equivalent diameter, and the signal propagates along with CSR without the attenuation [44,45]. During the test, it can be assumed that the surrounding environment does not affect the stress wave signal. From the derivation in the literature [42,43], it can be obtained:

$$f_n = \frac{nC}{2L} \tag{3}$$

This equation can be approximated as

$$\Delta f = f_{n+1} - f_n = \frac{C}{2L} \tag{4}$$

where f_n is the n-th resonance frequency; C is the stress wave velocity in CSRs; L is the length of CSRs; n is a constant (n = 0, 1, 2, 3, ⋯).

Through time-domain analysis, C and L can be determined, and then Δf can be obtained by Eq. (4). If Δf is approximately equal to the main frequency obtained by FFT, then the result of the time-domain judgement is reliable.

(1) Type I CSR impact echo test results

Figure 8 shows the measured time-domain waveform of A2 and A6 in Type I CSRs. There are significant reflected echoes from the top and bottom

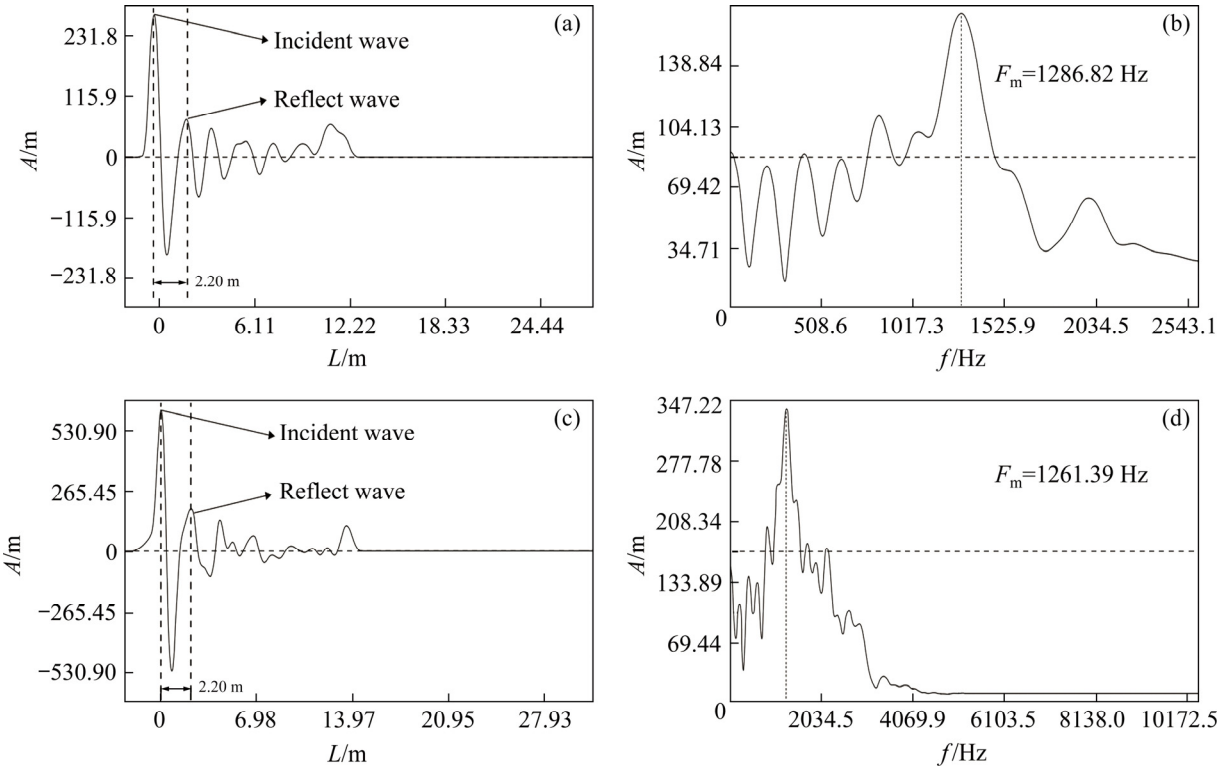

Fig. 8 Time (a, c) and frequency (b, d) domain waveforms detected in Type I CSRs: (a, b) A2 (Test site: production workshop; Wave velocity: 5093 m/s); (c, d) A6 (Test site: production workshop; Wave velocity: 5820 m/s)

Table 6 Wave velocity verified by attenuation coefficient

Specimen	Inversion wave velocity/(m·s^{-1})	Corrected wave velocity/(m·s^{-1})	Difference/%
A1	4825	4754.97	1.45
A2	5093	5094.61	−0.03
A3	5093	5126.96	−0.67
A4	5473	5612.16	−2.54
A5	5641	5563.64	1.37
A6	5820	5773.9	0.79

of CSRs, and there are no other reflected echoes between the top and bottom of CSRs. The waveform curves of A2 and A6 are complete and regular. The stress wave has multiple reflections at the top and bottom of CSRs, and the time interval between two adjacent peaks in the time-domain waveform is approximately equal. Further, the amplitude gradually attenuates. From the perspective of frequency-domain analysis, the fundamental frequency in the spectrum diagram of A2 is 1286.82 Hz, and $\Delta f = c/(2L) = 1157.00$ Hz; the fundamental frequency in the spectrum diagram of A6 is 1261.39 Hz, and $\Delta f = c/(2\mathrm{L}) = 1332.70$ Hz. The percentage of the difference between fundamental frequency and Δf is within 15%; therefore, the two CSRs are judged to be intact. The actual condition of the two CSRs after grooving also confirms this result, as shown in Fig. 9.

(2) Type II CSR impact echo test results

As the defects in CSR are filled with impurities such as aluminium liquid and electrolytes, the wave impedance decreases. When the stress wave propagates into the impurities, the reflected wave with the same phase as the incident wave is generated at the defects. The rest of the stress wave reaches the bottom of CSR through the impurity layer and is reflected back. Figure 10 shows the measured time-domain curve of the Type II CSRs. The reflection echo at the top and bottom of CSRs can be distinguished from the diagram, and the phases of the two are the same. From the time-domain curve, it can be concluded that the A7 has defects at approximately 1.01 m, and A8 has defects at approximately 0.94 m. Besides, there are two distinct peaks in the spectrum of A7 and A8. This is because the stress wave is partially reflected at the defect before reaching the bottom end of CSR,

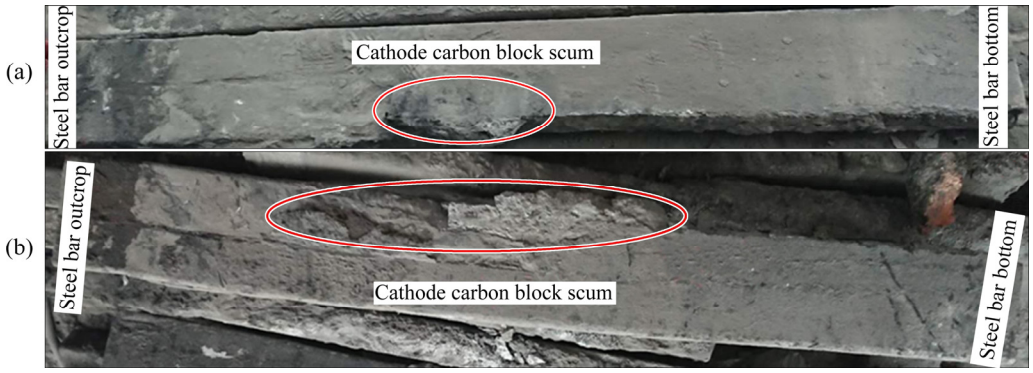

Fig. 9 Damaged condition of CSR: (a) A2; (b) A6

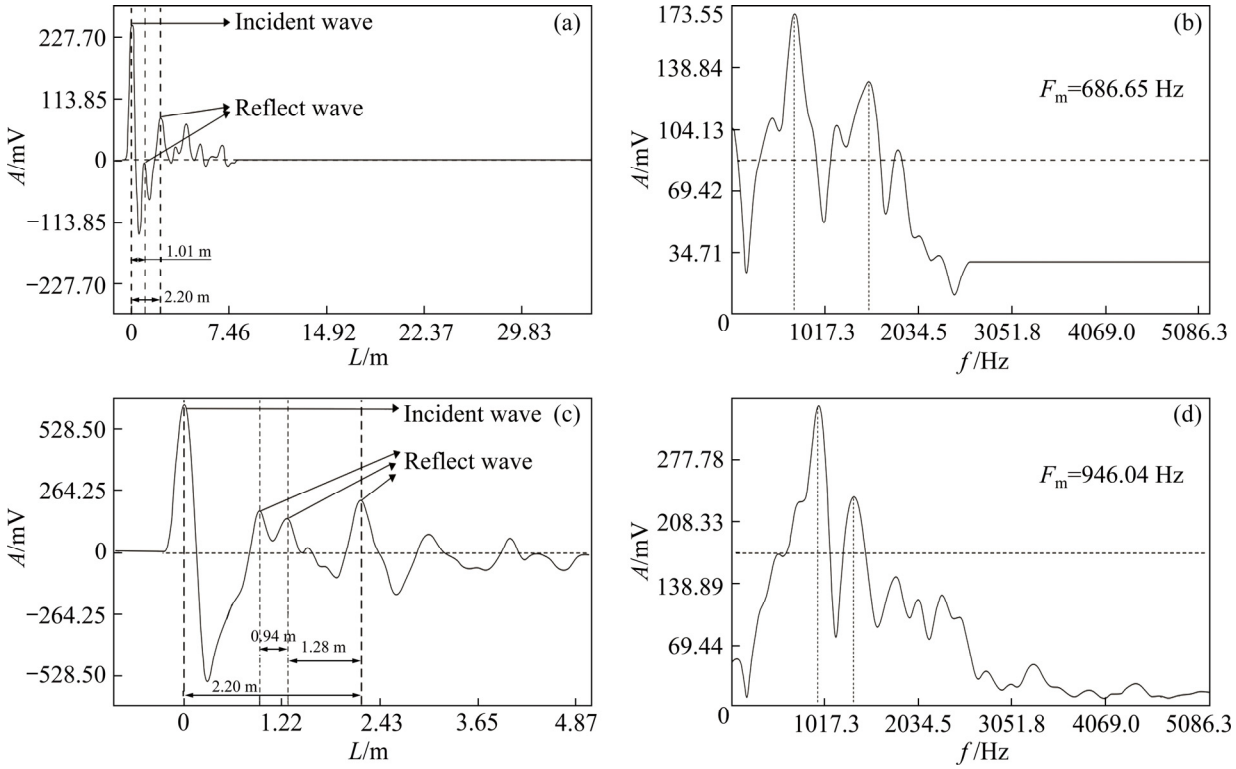

Fig. 10 Time (a, c) and frequency (b, d) domain waveform detected in Type II CSR: (a, b) A7 (Test site: production workshop; Wave velocity: 3107 m/s); (c, d) A8 (Test site: production workshop; Wave velocity: 2026 m/s)

resulting in the shortening of the reflection path of the stress wave. As shown in Fig. 10(b), the two obvious peak frequencies of A7 are 686.65 and 1525.00 Hz, and the corresponding depths are calculated to be 2.26 and 1.02 m by Eq. (4); two obvious peak frequencies of A8 are 946.04 and 1322.46 Hz, and the corresponding depths are calculated to be 1.07 and 0.76 m by Eq. (4), which is almost consistent with the defect position in time-domain analysis. Therefore, when the frequency of structural thickness drifts to the low-frequency part, the damage frequency drifts to the high-frequency is the main basis for damage judgment, which is consistent with the results of numerical simulation performed by ZHOU et al [46]. The locations of the defects in these two CSRs correspond to the locations of the defects in actual measurement after grooving, as shown in Fig. 11.

(3) Type III CSR impact echo test results

After the fusion of CSR, it is difficult to distinguish the reflection echo at the defect boundary and the bottom of CSR. Therefore, the stress wave velocity of CSR cannot be inverted according to the length. Because the part between the fracture position and the outcrop of CSR is

relatively intact, the wave velocity of A1 in Type I CSR is used to calculate the defect location. Figure 12 shows the measured time-domain waveform of Type III CSRs. It can be found that A9 is fused at 0.96 m and A10 is fused at 0.90 m, and the time difference between the two adjacent peaks is relatively close. Further, the amplitude gradually decreases, indicating that the stress wave is reflected back and forth on the fracture surface of CSR many times. From the perspective of frequency-domain analysis, the fundamental frequency in the spectrum of A9 is 2807.62 Hz and $\Delta f = c/(2L) = 2513.02$ Hz. The fundamental frequency in the spectrum of A10 is 2827.96 Hz and $\Delta f = c/(2L) = 2757.00$ Hz. The difference between the fundamental frequency and Δf is within 15%, indicating that the fracture location in the time-domain analysis is reliable. The actual fracture locations of the two CSRs after grooving also confirm this result, as shown in Fig. 13.

Table 7 gives the defect locations of CSRs detected by the impact echo method and the measurement after grooving. The results show that impact echo technology can effectively identify the defects and integrity of the CSRs with an error of less than 15%, and this technology can be applied to the integrity inspection of CSRs of the aluminium electrolyzer during service.

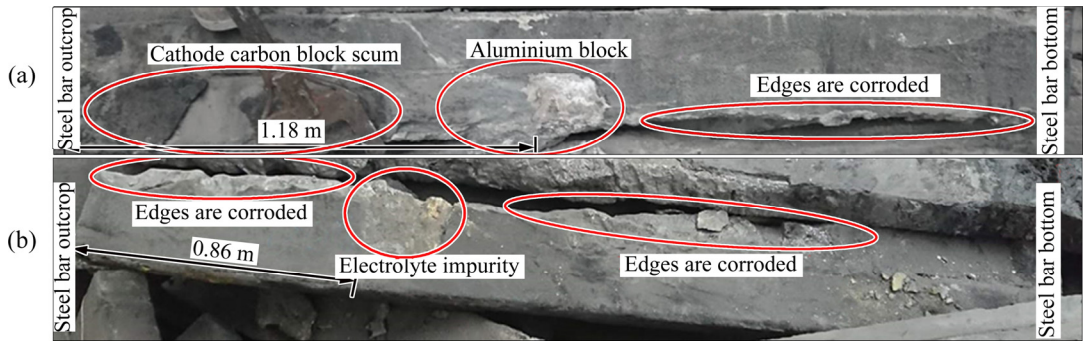

Fig. 11 Damaged condition of CSR: (a) A7; (b) A8

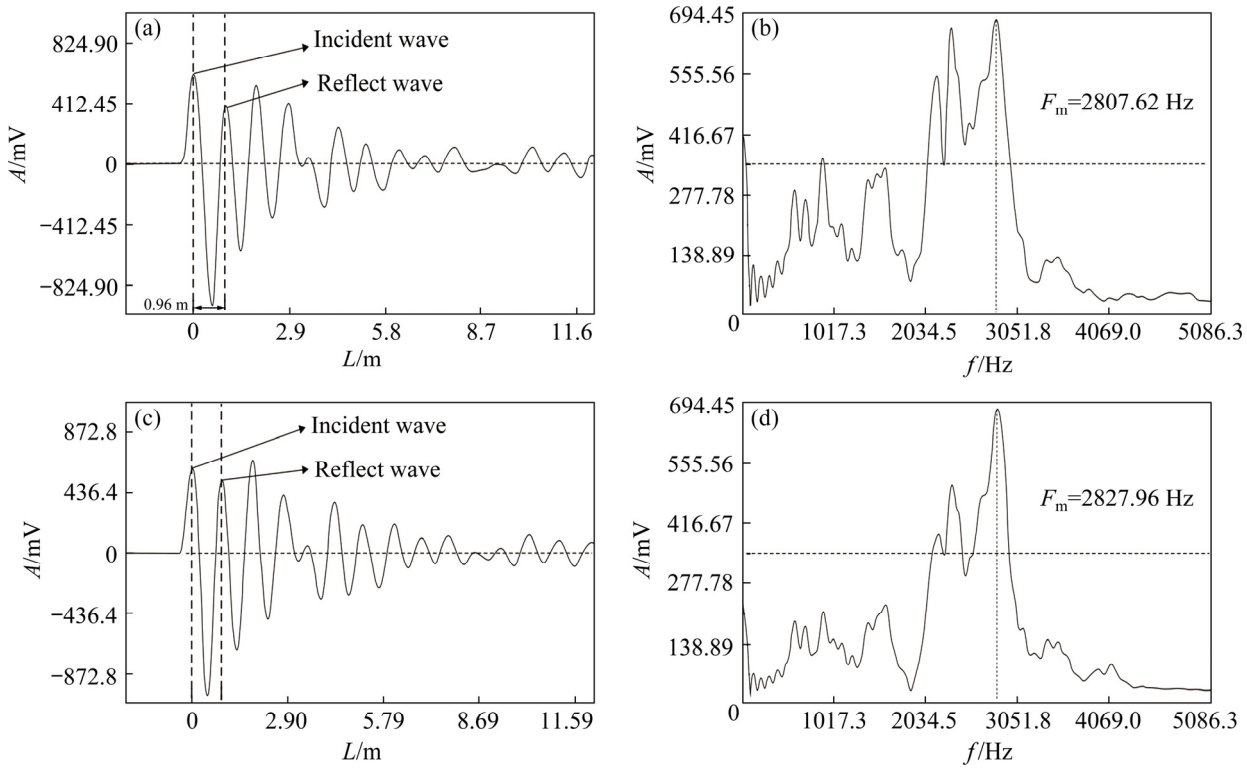

Fig. 12 Time (a, c) and frequency (b, d) domain waveforms detected in Type III CSRs: (a, b) A9 (Test site: production workshop; Wave velocity: 4825 m/s); (c, d) A10 (Test site: production workshop; Wave velocity: 4825 m/s)

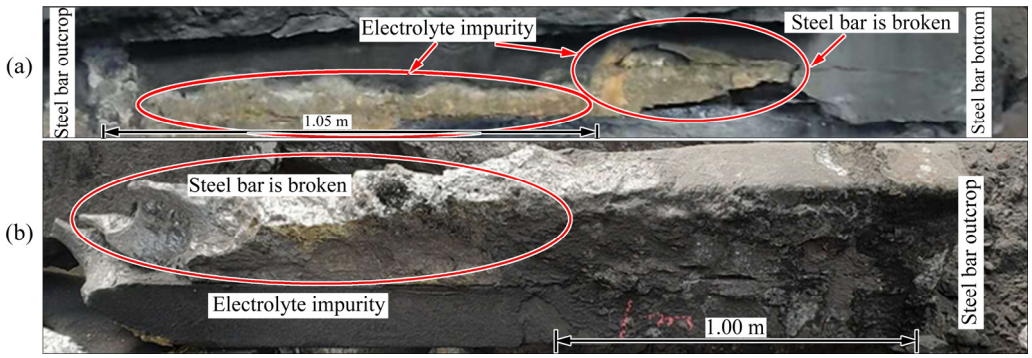

Fig. 13 Damaged condition of CSR: (a) A9; (b) A10

Table 7 Results of impact echo detection

Specimen	Wave velocity/ ($m \cdot s^{-1}$)	Defect location of impact echo detection/m	Actual defect location/m	Bottom position/m	Error/%	Integrity category
A1	4825.00	−	−	2.20	−	I
A2	5093.00	−	−	2.20	−	I
A3	5093.00	−	−	2.20	−	I
A4	5473.00	−	−	2.20	−	I
A5	5641.00	−	−	2.20	−	I
A6	5820.00	−	−	2.20	−	I
A7	3107.00	1.01	1.18	2.20	14.40	II
A8	2015.00	0.94	0.86	2.20	9.30	II
A9	4825.00	0.96	1.05	−	8.60	III
A10	4825.00	0.90	1.00	−	10.00	III

4 Conclusions

(1) Before the installation of CCB into the electrolyzer, sampling and drilling samples are generally required to evaluate the quality of the entire CCB. However, the traditional methods are random and cannot ensure the intact of the entire CCB. In this study, the combined evaluation method of wave velocity and voltage drop is proposed to evaluate CCB before installation into the electrolyzer and improve the service life of the electrolyzer. The study results indicate that the wave velocity of CCB has a strong correlation with other physicochemical parameters, and the combined test of voltage drop and wave velocity can be used to effectively assess the quality of the large-size CCBs.

(2) Due to the complexity of the electrolyzer (especially the influence of high temperature and electromagnetic radiation), many methods such as ultrasonic testing are not suitable for on-site CSRs defect detection. To some extent, electromagnetic interference can be avoided in defect detection by using mechanically excited elastic waves for defect detection. The impact echo technology is firstly applied to CSRs defect detection, and the results show that it can effectively assess the damage condition of CSRs and determine the location of defects. Nevertheless, due to the varying degrees of damage of CSRs in the electrolyzer, the response of various defects to the elastic wave with a specific frequency band is also different. In future research, elastic waves can be stimulated in different frequency bands to determine a specific frequency excitation wave suitable for a specific CSR evaluation.

Acknowledgments

The authors are grateful for the financial supports from the National Natural Science Foundation of China (No. 42172316), the Natural

Science Foundation of Hunan Province, China (No. 2021JJ30810), and the Research Fund of the State Key Laboratory of Coal Resources and Safe Mining, China (No. CUMT SKLCRSM21KF005).

References

[1] QIU Zhu-xian. Aluminum smelting in prebaked cell [M]. 3rd ed. Beijing: Metallurgical Industry Press, 2005. (in Chinese)

[2] WANG Jin-rong. Selection and control of heating system in high-temperature flue gas roasting process of aluminum electrolyzer [D]. Changsha: Central South University, 2005. (in Chinese)

[3] LÜ Xiao-jun, ZHANG Heng-xing, HAN Ze-xun, WANG Kang-jie, GUAN Chao-hong, SUN Qi-dong. Numerical simulation of coupled thermo-electrical field for 20 kA new rare earth reduction cell [J]. Transactions of Nonferrous Metals Society of China, 2020, 30(4):1124−1134.

[4] HOU Wen-yuan, LI He-song, LI Mao, CHENG Ben-jun, FENG Yuan. Effects of electrolysis process parameters on alumina dissolution and their optimization [J]. Transactions of Nonferrous Metals Society of China, 2020, 30(12): 3390−3403.

[5] ZHU Jun, XUE Ji-lai, ZHANG Ya-nan, LI Xiang, CHEN Tong. Ambient electrical conductivity of carbon cathode materials for aluminum reduction cells [J]. Transactions of Nonferrous Metals Society of China, 2015, 25(11): 3753−3759.

[6] YANG Shuai, LI Jie, ZHANG Hong-liang, ZOU Zhong, LAI Yan-qing. Numerical simulation of heat transfer coefficient between bath and lining in aluminum reduction cell [J] The Chinese Journal of Nonferrous Metals, 2017, 27(1): 162−170. (in Chinese)

[7] LI Ping, YU Li-qun, LI Wan-qiu. Homogeneous quality of carbon products and ultrasonic sound velocity detection [J]. Carbon, 2002, 2: 41−43. (in Chinese)

[8] XIANG Yuan-bo, XIAO Lin-xiu, LIAN Jing-huo. Analysis of echo height using broadband probes in ultrasonic testing of high-attenuation materials [J]. Nondestructive Testing, 1995, 3: 28−34. (in Chinese)

[9] LI Ping, LU Yu-jun, LI Wan-qiu. The application of X-ray and ultrasonic detection methods in carbon graphite products [J]. Nondestructive Testing, 1999, 3:1−5. (in Chinese)

[10] FOOSENACE T, JARCK S, OKSEFJELL T, ΦYE H A, WANG Shu. Using ultrasonic to control the quality of cathode carbon block [J]. Carbon Techniques, 1992(2): 39−41. (in Chinese)

[11] SHI Zhong-ning, REN Bi-jun, LIU Shi-ying, QIU Zhu-xian. Investigation of the failure of a 300 kA prebaked anode reduction cell [J]. GALLOWAY J T. Aluminum Reduction Technology 2006. Saint Antonio, PA: TMS, 2006: 313−317.

[12] HAUPIN W E. Cathode voltage loss in aluminum smelting cells [C]//GEOFF B. Aluminum Reduction Technology, 2013. Marc Dupuis and Gary Tarcy, PA: TMS, 2013: 147−152.

[13] MICHEL C. Evolution of the cathode ohmic drop during the electrolysis in the aluminum cell [C]//Light Metals. Mew York: TMS, 1985: 989−1003.

[14] SORIE M, GRAN H. Cathode collector bar-to-carbon contact resistance [C]//CUTSHALL E R. Light Metals 1992. San Diego, California, PA: TMS, 1992: 779−787.

[15] LI Shi-jun. Damage detection, judgment and maintenance of large prebaked aluminum electrolyzer [J]. Non-Ferrous Metals (Smelting Part), 1999, 3: 33−38. (in Chinese)

[16] ZHAO Qun, XIE Yan-li, GAO Bing-liang, QIU Zhu-xian, ZHAO Wu-wei. Chemical reaction model of cathode failure in large prebaked anode aluminum reduction cells [J]. Transactions of Nonferrous Metals Society of China, 2002, 12(6): 1195−1198.

[17] RAFIEI P, HILTMANN F, HYLAND M, JAMES B, WELCH B. Electrolyte degradation within cathode materials [C]//TOMSETT A, JOHNSON J. Electrode Technology for Aluminum Production 2013. PA: TMS, 2013: 1011−1016.

[18] KRAUTKRÄMER J. Determination of the size of defects by the ultrasonic impulse echo method [J]. British Journal of Applied Physics, 2002, 10(6): 240−245.

[19] FELICE M V. Ultrasonic array inspections for complex defects [D]. Bristol: University of Bristol, 2015.

[20] SILK M G, LIDINGTON B H. Defect sizing using an ultrasonic time delay approach [J]. British Journal of Non-destructive technology (March), 1975(3): 33−36.

[21] SILK M G, LIDINGTON B H. The potential of scattered or diffracted ultrasound in the determination of crack depth [J]. Non-Destructive Test, 1975, 8(3): 146−151.

[22] SILK M G. The transfer of ultrasonic energy in the diffraction technique for crack sizing [J]. Ultrasonics, 1979: 113−121.

[23] RAVENSCROFT F A, NEWTON K, SCRUBY C B. Diffraction of ultrasound by cracks: Comparison of experiment with theory [J]. Ultrasonics, 1991, 29 (1): 29−37.

[24] BULLEIT W M, FALK R H. Modeling stress wave passage times in wood utility poles [J]. Wood Science and Technology, 1985, 19(2): 183−191.

[25] WANG X P, ROSS R J, BRASHAW B K, PUNCHES J, ERICKSON J R, FORSMAN J W, PELLERIN R E. Diameter effect on stress-wave evaluation of modulus of elasticity of small diameter logs [J]. Wood and Fiber Science, 2004, 36(3): 368−377.

[26] WANG X P. Acoustic measurements on trees and logs: A review and analysis [J].Wood Science and Technology, 2013, 47(5): 965−975.

[27] NIA Sheng-huoo, YANG Yu-zhang, TSAC Pei-hsun, CHOU Wei-hsiang. Evaluation of pile defects using complex continuous wavelet transform analysis [J]. NDT & E International, 2017, 87: 50−59.

[28] HSIAO Chiamen, CHENG Chia-chi, LIOU Tzunghao, JUANG Yuanting. Detecting flaws in concrete blocks using the impact-echo method [J]. NDT & E International, 2008, 41: 98−107.

[29] MONTIEL-ZAFRA V, CANADAS-QUESADA V, CAMPOS-SUNOL M J, VERA-CANDEAS P, RUIZ-REYES N. Monitoring the internal quality of ornamental stone using impact-echo [J]. Applied Acoustics, 2019, 155: 180−189.

[30] WANG Chung-yue, CHIU Chin-lung, TSAI Kun-yi, CHEN Pi-kuan, PENG Peng-chi, WANG Hao-lin. Inspecting the

current thickness of a refractory wall inside an operational blast furnace using the impact echo method [J]. NDT & E International, 2014, 66: 43−51.
[31] SADRI A, TIMMER R. Blast furnace non-destructive testing (NDT) for defect detection and refractory measurements [C]//AISTech 2006. Cleveland: Association for Iron & Steel Technology, 2006: 593−602.
[32] SADRI A, WALTERS G. Determination of refractory and castable quality in operating industrial furnaces, using a stress wave reflection technique [C]//ALFANTAZI A, GU G P, ELBOUJDAINI M. Proceedings of 44th Annual Conference of Metallurgists. Calgary, Canada: Metallurgy and Materials Society of CIM, 2005: 357−385.
[33] YAO Fei, CHEN Guan-yu, ABULA A. Research on signal processing of segment-grout defect in tunnel based on impact-echo method [J]. Construction and Building Materials, 2018, 187: 280−289.
[34] DAI Yu-wen. Reliability method of solid concrete-soil pile damage identification based on low strain reflected wave method [D]. Wuhan: Huazhong University of Science and Technology, 2018. (in Chinese)
[35] JEONG H, HSU D K. Experimental analysis of porosity-induced ultrasonic attenuation and velocity change in carbon composites [J]. Ultrasonics, 1995, 33(3):195−203.
[36] POPOVICS J S, SONG W, ACHENBACH J D, LEE J H, ANDRE R F. One-sided stress wave velocity measurement in concrete [J]. Journal of Engineering Mechanics, 1998, 124(12): 1346−1353.
[37] WYLLIE M R J, GREGORY A R, GARDNER, G H F. An experimental investigation of factors affecting elastic wave velocities in porous media [J]. Geophysics, 1958, 23(3): 459−493.
[38] LI Guang-hui, WENG Xiang, DU Xiao-cheng, WANG Xi-ping, Feng Hai-lin. Stress wave velocity patterns in the longitudinal–radial plane of trees for defect diagnosis [J]. Computers and Electronics in Agriculture, 2016, 124: 23−28.
[39] KONDRATENKO A M, NERSESOV I L. Some results of the study on change in the velocities of longitudinal and transverse waves in a focal zone [J]. Trudy Inst Fiz Zemli, 1962, 25: 130−150.
[40] LIU Xi-ling, HAN Meng-si, LI Xi-bing, CUI Jia-hui, LIU Zhou. Elastic wave attenuation characteristics and relevance for rock microstructures [J]. Journal of Mining Science, 2020, 56: 215−225.
[41] FUTTERMAN W I. Dispersive body waves [J]. Journal of Geophysical Research, 1962, 67(13): 5279−5291.
[42] XU You-zai. New technology of dynamic measurement of piles [M]. 2nd ed. Beijing: China Building Industry Press. (in Chinese)
[43] KOTEN H V, MIDDENDORP P, BREDERODE P V. An analysis of dissipative wave propagation in a pile [C]//International Seminar on the Application of Stress Wave Theory on Piles. Stockholm, Sweden, 1980.
[44] ANDERSON S P. Higher-order rod approximations for the propagation of longitudinal stress waves in elastic bars [J]. Journal of Sound and Vibration, 2006, 290(1−2): 290−308.
[45] YANG Ke. A unified solution for longitudinal wave propagation in an elastic rod [J]. Journal of Sound and Vibration, 2008, 314(1−2): 307−32.
[46] ZHOU Chang-sheng, WANG Ping, HU Zhi-peng, ZHU Hao. Numerical simulation of impact-echo method identify the depth of honeycomb damage in unballasted track [J]. Applied Mechanics and Materials, 2014, 584−586: 2060−2067.

基于无损检测技术的铝电解槽阴极质量及破损评估

罗 雨[1]，李生相[1]，陈道龙[1]，刘希灵[1]，马春德[2]，李夕兵[1]

1. 中南大学 资源与安全工程学院，长沙 410083；
2. 中南大学 高等研究中心，长沙 410083

摘 要：为评估电解槽阴极质量及其破损状况，运用声波检测技术与冲击回波检测技术对电解槽阴极部分进行检测。结果表明：入槽前阴极炭块中波速与孔隙率、密度倒数的开方间存在线性关系，并通过声波−电压降联合测试结果找出质量相对良好的阴极炭块；此外，利用冲击回波检测技术对阴极钢棒进行现场检测，结果表明其可有效评估阴极钢棒的破损状况，并实现破损部位定位。提出一种全新的、可量化的阴极质量及破损评估方法，可为电解槽生命周期延长及评价提供参考。

关键词：电解槽；波速检测；冲击回波技术；阴极质量；破损评估

(Edited by Bing YANG)